


 Cite this: *RSC Adv.*, 2024, 14, 20454

# Copper–Vit B<sub>3</sub> MOF preparation, characterization and catalytic evaluation in a one-pot synthesis of benzoxanthenones with docking validation as anti *H. pylori*†

 Asma S. Al-Wasidi,<sup>a</sup> Mahmoud Tarek,<sup>\*b</sup> Gehad E. Said,<sup>ib</sup> <sup>\*b</sup> Ahmed M. Naglah,<sup>\*c</sup> Abdulrahman A. Almehizia<sup>ib</sup> <sup>c</sup> and Tamer K. Khatab<sup>d</sup>

Copper–Vit B<sub>3</sub> MOF was successfully prepared by efficient and eco hydrothermal method. The prepared MOF was characterized as a tetragonal crystal copper-MOF nanoparticles by FTIR, SEM, TEM, EDX and XRD. The prepared nanoparticles were used as an effective, inexpensive and low-toxic catalyst in the one-pot synthesis of some new benzoxanthenone derivatives. As example 4-(9,9-dimethyl-11-oxo-8,10,11,12-tetrahydro-9H-benzo[a]xanthen-12-yl)phenyl benzoate (**4h**) was synthesized in high yield 92%. The MOF catalyst's role is activating the nucleophilic attack by increasing the carbonyl polarization, and this generally improves the reaction time, which ranges between 20–60 minutes and products' yields ranging between 80–92%. Prepared compounds (**4a–4j**) undergo molecular docking scanning as *Helicobacter pylori* type II dehydroquinase inhibitors, and the data obtained showed that there are three promises of the prepared compounds **4d**, **4e**, **4h** and **4j** compared with amoxicillin.

 Received 10th May 2024  
 Accepted 16th June 2024

DOI: 10.1039/d4ra03468f

[rsc.li/rsc-advances](https://rsc.li/rsc-advances)

## 1. Introduction

Xanthene, which is an annulated pyran heterocyclic compound, is one of the most applicable compounds in organic chemistry, and it is presented as a scaffold in a lot of natural products,<sup>1–3</sup> fluorescent dyes and many bioactive compounds<sup>4</sup> (Fig. 1). Due to the presence of the pyran framework, various biological functions have been recognized for them, such as antimicrobial, antiviral, analgesic, anticancer, antioxidant, antimalarial and anti-inflammatory.<sup>5–11</sup> They also can be used as sensitizers in photodynamic therapy,<sup>12</sup> in the visualization of biomolecules as chemical probes<sup>13</sup> and in industrial materials.<sup>14</sup> The xanthine scaffold has been introduced into many important therapeutic compounds (Fig. 1). Synthetic methods that use less harmful materials and find applications that are useful for society's well-being are in tremendous demand right now. Following green

chemistry principles to create ecologically sustainable processes is a major issue for chemists.<sup>15</sup> The catalysis process involves accelerating a chemical reaction by including a catalyst.<sup>16</sup>

Three or more chemical reagents reacting in a single pot to form a new product is known as a multicomponent reaction (MCR). Due to their ability to synthesize some important organic compounds and structures in a one-pot single reaction, MCRs have drawn attention in the fields of synthesis and medicinal chemistry.<sup>17,18</sup> These reactions produce very selective products in addition to requiring less energy and solvent. Owing to the multiple benefits of the MCR process, the development of innovative, eco-friendly, and MOF-catalyzed MCR processes has been seen as an intriguing, rapidly expanding area of study in organic chemistry.<sup>19,20</sup> Metal–Organic Frameworks (MOFs) represent a fascinating class of materials that have gained significant attention for their potential applications across various fields, including organic synthesis, gas storage, sensors and biomedical applications.<sup>21–26</sup> These crystalline compounds consist of metal ions or clusters coordinated to organic ligands to form one-, two-, or three-dimensional structures.<sup>27–29</sup> MOFs have a lot of unique properties that mean they are expected to play an increasingly important role in the development of efficient, selective, and sustainable catalytic processes in organic chemistry. The high surface areas and presence of catalytically active sites contribute to their high catalytic efficiency, tunable pore sizes as designing MOFs with specific pore sizes allows for the selective inclusion or exclusion of molecules, and chemical

<sup>a</sup>Department of Chemistry, College of Science, Princess Nourah Bint Abdulrahman University, Riyadh 11671, Saudi Arabia. E-mail: [asalwasidi@pnu.edu.sa](mailto:asalwasidi@pnu.edu.sa)
<sup>b</sup>Chemistry Department, Faculty of Science, Mansoura University, 35516 Mansoura, Egypt. E-mail: [gehadsaid@mans.edu.eg](mailto:gehadsaid@mans.edu.eg); [mahmoudtarek.tm@gmail.com](mailto:mahmoudtarek.tm@gmail.com)
<sup>c</sup>Drug Exploration and Development Chair (DEDC), Department of Pharmaceutical Chemistry, College of Pharmacy, King Saud University, P. O. Box 2457, Riyadh 11451, Saudi Arabia. E-mail: [anaglah@ksu.edu.sa](mailto:anaglah@ksu.edu.sa); [mehizia@ksu.edu.sa](mailto:mehizia@ksu.edu.sa)
<sup>d</sup>Organometallic and Organometalloid Chemistry Department, National Research Centre, 33 ElBehouth St., Dokki, 12622 Giza, Egypt. E-mail: [Tamer\\_khatab@hotmail.com](mailto:Tamer_khatab@hotmail.com)

 † Electronic supplementary information (ESI) available. See DOI: <https://doi.org/10.1039/d4ra03468f>

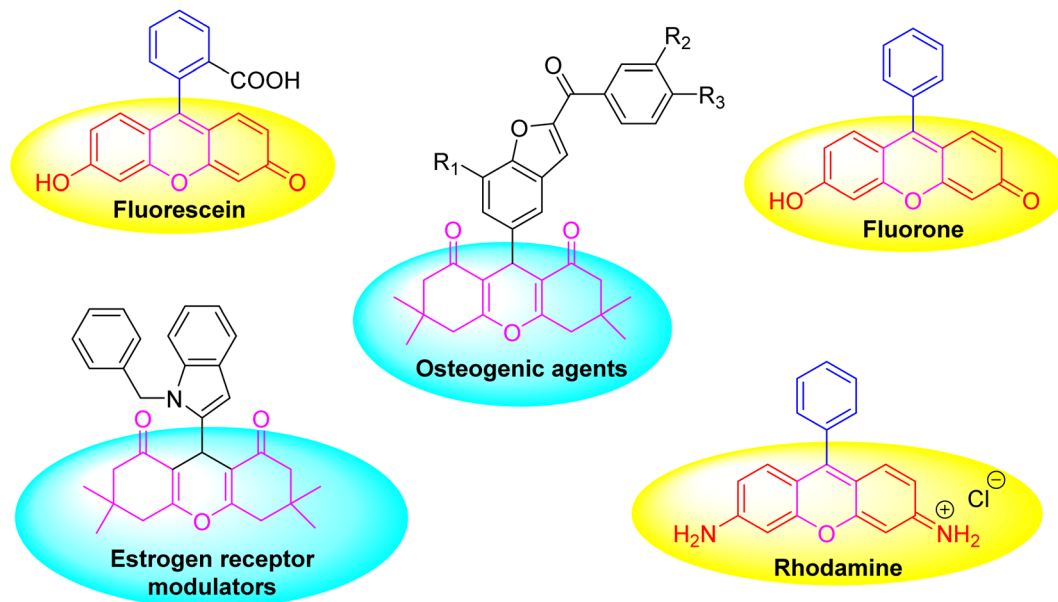



Fig. 1 Representative examples for some biologically important xanthene nuclei and xanthene dyes.

stability are crucial for MOFs use in harsh reaction conditions.<sup>30,31</sup>

In this study, we have prepared a novel copper-based MOF material (Cu-Vit B<sub>3</sub>) with nano structure, using a native biomolecules of vitamin B<sub>3</sub> as an organic ligand. Synthesized ligands undergo docking validation as *Helicobacter pylori* type II dehydroquinase inhibitor. One of the most common modern diseases these days is stomach bacteria, and this is due to the pollution of food. *Helicobacter pylori* (*H. pylori*) is a spiral shaped a Gram-negative bacterium that lives and multiplies in the lining of the stomach, and it is a common cause of many stomach diseases including peptic ulcers.<sup>32,33</sup>

## 2. Experimental

### 2.1. Materials

Vitamin B<sub>3</sub>, copper(II) acetate monohydrate, ethylene glycol, ethanol and deionized water (DI) were purchased from Sigma Aldrich and used directly without purification.

### 2.2. Catalyst preparation

In a 50 mL beaker, vitamin B<sub>3</sub> (0.123 g, 1 mmol) was dissolved in 20 mL of ethylene glycol and in another beaker copper(II) acetate monohydrate (0.1 g, 0.5 mmol) was dissolved in 20 mL of ethylene glycol, then heated at 80 °C and stirred for 10 min respectively. Then copper(II) acetate monohydrate solution was rapidly added to the vitamin B<sub>3</sub> solution with fast stirring at 1500 rpm for 10 min. Subsequently, the solution was transferred to a Teflon-lined hydrothermal autoclave set at 180 °C for two days. The mixture was then centrifuged at 7000 rpm and washed three times with 60 °C DI water and absolute ethanol to produce cyan powders of Cu-Vit B<sub>3</sub>-MOF.

These were then freeze-dried and kept at 4 °C for additional research.

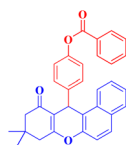
### 2.3. Characterization of the catalyst

The surface morphology and composition of the catalyst were deduced using a Jeol-JSM-6510LV scanning electron microscope (SEM) and energy dispersive X-ray spectroscopy (EDX), respectively. The particles size was produced from transmission electron microscopy (TEM) using a JEOL-JEM-2100 at 200 kV to acquire X-ray powder diffraction patterns (XRD); the Ni-filtered Cu K $\alpha$  radiation = 1.540 at 40 kV, 30 mA, and a scanning range  $2\theta$  of 5–80 was employed. By using a Mattson 5000 FT-IR spectrophotometer at room temperature we obtained FT-IR spectra of Cu-MOF through creating a disc of it with 0.1 g KBr.<sup>34</sup>

### 2.4. Organic reaction and structure identification

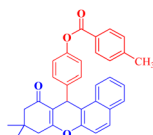
**General procedure for the synthesis of benzoxanthene derivatives (4a–j) catalyzed by Cu-MOF.** To a mixture of one mmol dimedone (1; 0.14 g), one mmol  $\beta$ -naphthol (2; 0.144 g) and one mmol aromatic aldehyde (3a–j) a catalytic amount of Cu-MOF (0.05 g) was added. The mixture was stirred at 60–70 °C. The reaction was monitored by chromatographic TLC till the reaction was completed. After the specified time has elapsed, the reaction is allowed to cool to room temperature, and the final product was extracted by ethyl acetate (20 mL). The MOF catalyst was removed by simple filtration. The solvent was evaporated *in vacuo*, and the crude residue product was washed with cold methanol to afford pure benzoxanthenones 3a–j in high yields. The spectral data of known benzoxanthenones (4a–g) are reported in the literature.<sup>35,36</sup> Moreover, the structures of the new derivatives (4h–j) were illustrated and discussed as follows.

4-(9,9-Dimethyl-11-oxo-8,10,11,12-tetrahydro-9H-benzo[a]xanthen-12-yl)phenyl benzoate (**4h**).



White solid;  $R_f = 0.60$  (8 : 2 petroleum ether/EtOAc); mp = 180–182 °C;  $^1\text{H NMR}$  (400 MHz,  $\text{CDCl}_3$ )  $\delta$  ppm: 1.132 (s, 3H,  $\text{CH}_3$ ), 1.256 (s, 3H,  $\text{CH}_3$ ), 2.32–2.51 (m, 4H,  $2\text{CH}_2$ ), 5.56 (s, 1H,  $\text{CH}_{\text{pyran}}$ ), 7.16–7.67 (m, 13H, Ar–H), and 8.20 (d,  $J = 7.6$  Hz, 2H, Ar–H).  $^{13}\text{C NMR}$  (100 MHz,  $\text{CDCl}_3$ )  $\delta$  ppm: 27.40, 29.66, 31.44, 32.47, 46.45, 47.08, 115.52, 121.38, 127.88, 128.57, 129.68, 129.82, 130.17, 133.53, 135.72, 148.95, 165.12, 189.42, and 190.55. Analysis for  $\text{C}_{32}\text{H}_{26}\text{O}_4$  (474.18): calculated: C, 80.99; H, 5.52%. Found: C, 80.92; H, 5.45%.

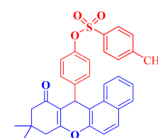
4-(9,9-Dimethyl-11-oxo-8,10,11,12-tetrahydro-9H-benzo[a]xanthen-12-yl)phenyl 4-methylbenzoate (**4i**).



White solid;  $R_f = 0.50$  (8 : 2 petroleum ether/EtOAc); mp = 185–187 °C;  $^1\text{H NMR}$  (400 MHz,  $\text{CDCl}_3$ )  $\delta$  ppm: 1.00 (s, 3H,  $\text{CH}_3$ ), 1.24 (s, 3H,  $\text{CH}_3$ ), 2.34–2.54 (m, 7H,  $2\text{CH}_2$ ,  $\text{CH}_3$ ), 5.66 (s, 1H,  $\text{CH}_{\text{pyran}}$ ), and 7.12–8.17 (m, 14H, Ar–H).  $^{13}\text{C NMR}$  (100 MHz,  $\text{CDCl}_3$ )  $\delta$  ppm: 21.80, 27.15, 29.32, 31.40, 32.56, 46.96, 50.43, 109.59, 115.54, 118.40, 121.65, 123.28, 126.37, 127.85, 128.06, 129.42, 129.70, 130.43, 131.45, 133.91, 135.74, 144.69, 145.20, 149.13,

154.50, 155.91, 164.86, 165.74, and 191.69. Analysis for  $\text{C}_{33}\text{H}_{28}\text{O}_4$  (488.20): calculated: C, 81.13; H, 5.78%. Found: C, 81.11; H, 5.71%.

4-(9,9-Dimethyl-11-oxo-8,10,11,12-tetrahydro-9H-benzo[a]xanthen-12-yl)phenyl 4-methylbenzenesulfonate (**4j**).



White solid;  $R_f = 0.60$  (8 : 2 petroleum ether/EtOAc); mp = 170–172 °C;  $^1\text{H NMR}$  (400 MHz,  $\text{CDCl}_3$ )  $\delta$  ppm: 0.95 (s, 3H,  $\text{CH}_3$ ), 1.14 (s, 3H,  $\text{CH}_3$ ), 2.24–2.35 (m, 2H,  $\text{CH}_2$ ), 2.40 (s, 3H,  $\text{CH}_3$ ), 2.57 (s, 2H,  $\text{CH}_2$ ), 5.70 (s, 1H,  $\text{CH}_{\text{pyran}}$ ), 6.79 (d, 2H,  $J = 6.4$  Hz, Ar–H), 7.16 (d, 2H,  $J = 6.4$  Hz, Ar–H), 7.25 (d, 2H,  $J = 6.4$  Hz, Ar–H), 7.32 (d, 1H,  $J = 8$  Hz, Ar–H), 7.43 (s, 2H, Ar–H), 7.55 (d,  $J = 5.6$  Hz, 2H, Ar–H), and 7.79–7.855 (m, 3H, Ar–H).  $^{13}\text{C NMR}$  (100 MHz,  $\text{CDCl}_3$ )  $\delta$  ppm: 21.69, 26.96, 29.36, 32.26, 34.07, 41.36, 50.85, 113.79, 117.07, 122.08, 123.50, 125.05, 127.04, 128.43, 128.52, 129.15, 129.58, 131.20, 131.53, 132.26, 143.63, 145.15, 147.85, 164.17, and 196.85. Analysis for  $\text{C}_{32}\text{H}_{28}\text{O}_5\text{S}$  (524.18): calc.: C, 73.26; H, 5.38; S, 6.11%. Found: C, 73.18; H, 5.30; S, 6.02%.

## 2.5. Molecular docking data

The targeted protein II dehydroquinase (DHQase) 3D crystal structure was downloaded from the PDB web site <https://www.rcsb.org/> (PDB ID 2c4w). The downloaded pdb file underwent some simple modification using MOE 2015.10 software starting by protein quick preparation and optimization, and then, additional water molecules were removed.

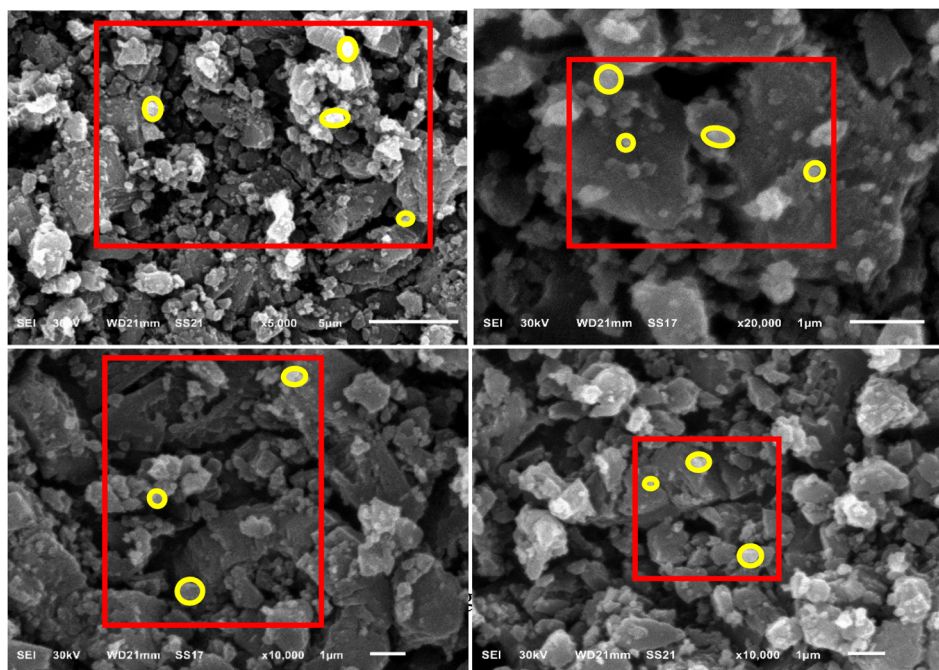


Fig. 2 SEM images of Cu/Vit  $\text{B}_3$ -MOF.



### 3. Results and discussion

#### 3.1. SEM analysis

Cu/Vit B<sub>3</sub>-MOF nanoparticle surface morphology appeared as nanospheres as obtained by SEM analysis (Fig. 2) and confirmed by TEM (Fig. 4).

#### 3.2. EDX elemental analysis

Using EDX, the elemental analysis of Cu-MOF was assessed, and it was determined that there were equivalent amounts of

nitrogen, carbon, oxygen, copper and some traces of zinc impurity, as illustrated in Fig. 3.

#### 3.3. TEM analysis

The TEM pictures of Cu-MOF, displayed in Fig. 4, demonstrate a spherical architecture with varying particle sizes ranging from 65 to 135 nm. The size of the MOF particles is inversely related to their surface area/volume ratio, so this variation will have an effective role in improving the catalytic activity.<sup>37</sup> The images were obtained at varied magnifications between 50 and 100 nm.

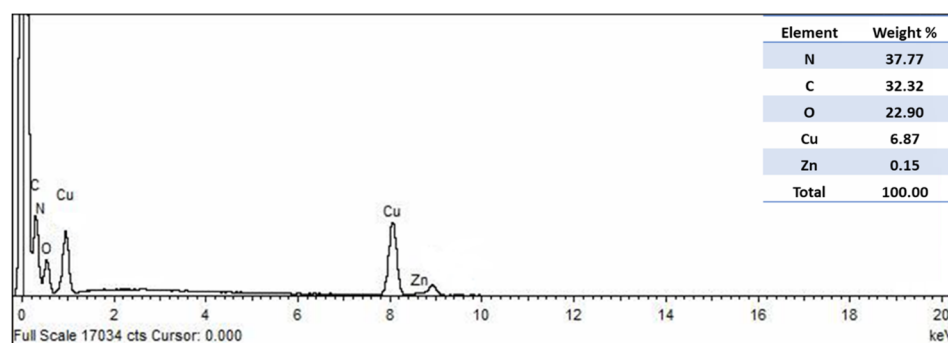


Fig. 3 EDX elemental analysis of Cu-MOF.

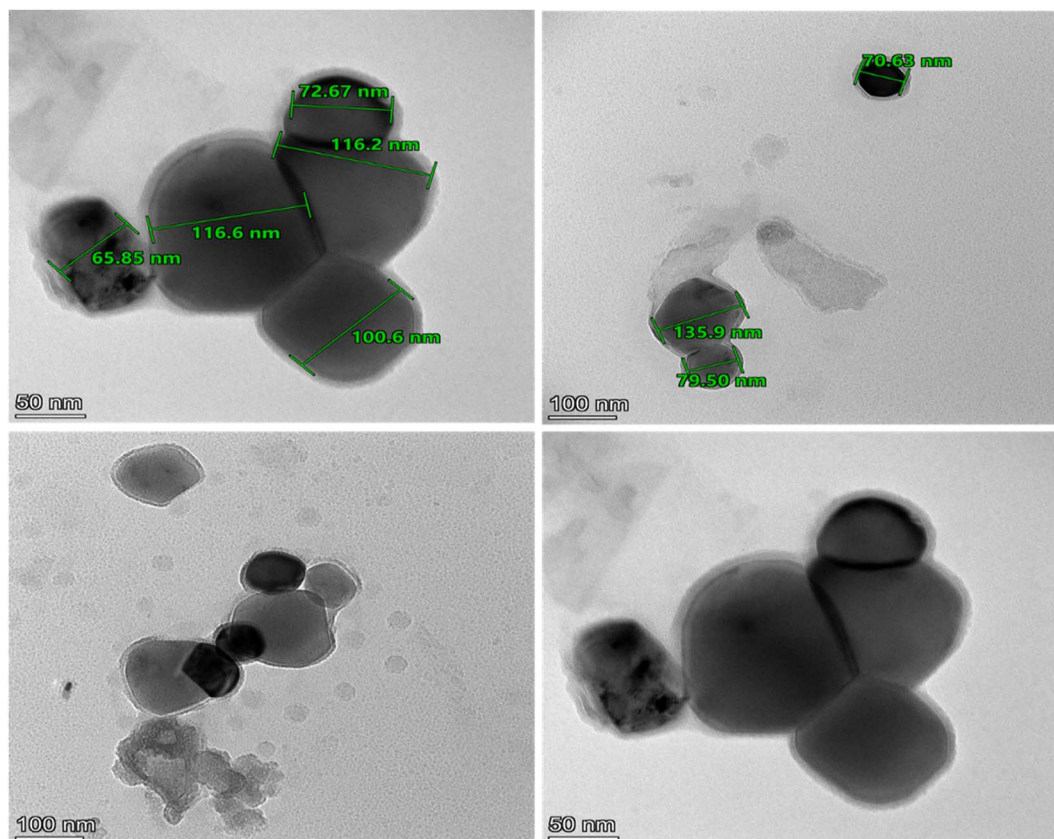
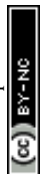


Fig. 4 TEM images of Cu/Vit B<sub>3</sub>-MOF.



Numerous benefits are introduced by this diverse array of nanosphere architectures, such as a massive surface area, biological activity, and catalytic activity.

### 3.4. XRD experimental data

The XRD spectrum revealed that Cu/Vit B<sub>3</sub>-MOF demonstrated relative peaks at 13.3, 14.9, 21.2, 23.1, 24.2, 26.9 and 36.9° (Fig. 5) which are characteristic of a tetragonal structure and show little deviation from simulated data. The proposed 3D-ball-stick structure of Cu/Vit B<sub>3</sub>-MOF (Fig. 6) reveals that the Cu atom bonded with two Vit B<sub>3</sub> molecules *via* a -COOH group side in one molecule and *via* a N atom of the other molecule and further repeating the pattern regularly to deduce the Cu-MOF crystal lattice.

### 3.5. Theoretical single crystal study

A hypothetical shape for the Cu/Vit-B<sub>3</sub>-MOF single crystal structure is shown in Fig. 7a, which was deduced from theoretical investigations using XRD data. Fig. 7b shows the full crystal image of Cu-MOF, which crystallizes in tetragonal structure with a high surface area and porosity.

### 3.6. Fourier transforms infrared (FTIR) spectra

By comparing the FTIR spectra of Cu-MOF and Vit B<sub>3</sub> (Fig. 8), the three bands at 1027, 1418 and 1700 cm<sup>-1</sup> characteristic for

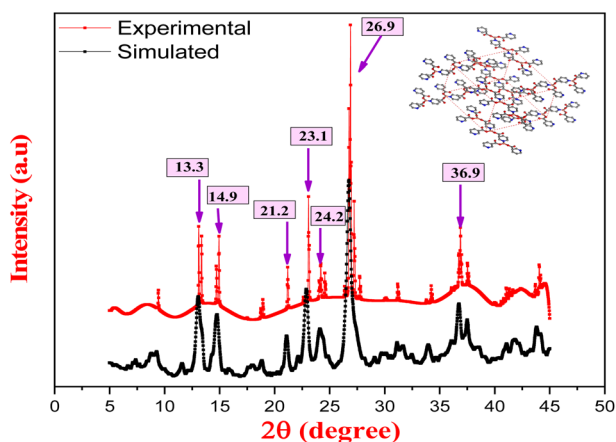


Fig. 5 XRD of Cu/Vit B<sub>3</sub>-MOF.

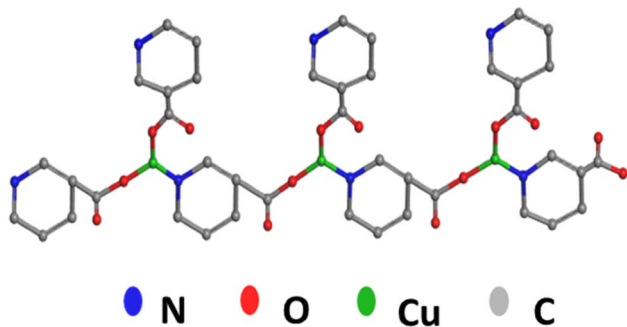


Fig. 6 Suggested ball-stick model for Cu/Vit-B<sub>3</sub>-MOF.

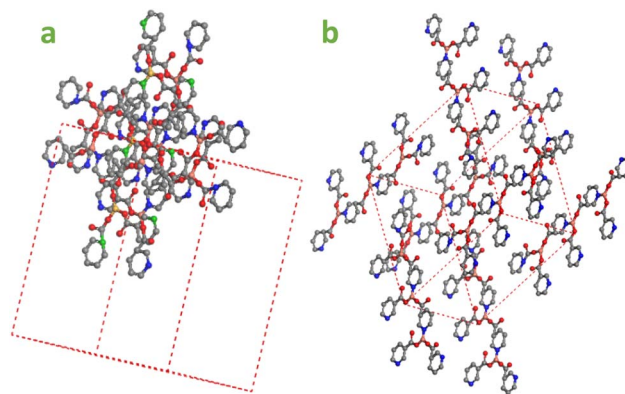


Fig. 7 (a) Single crystal structure of Cu/Vit-B<sub>3</sub>-MOF and (b) full crystal image.

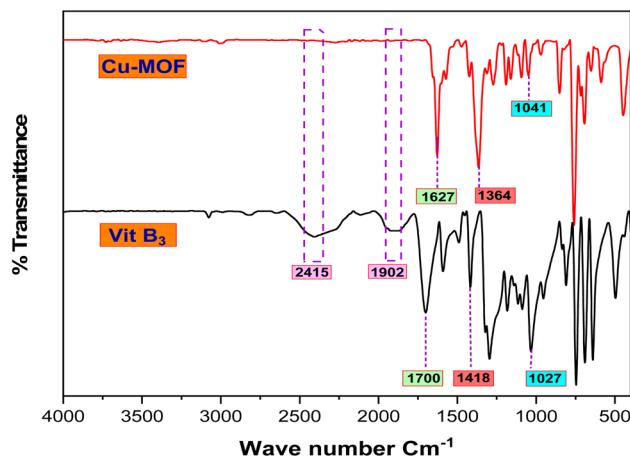


Fig. 8 FTIR spectrum of Cu/Vit B<sub>3</sub>-MOF.

$\nu(\text{C}-\text{C})$ ,  $\nu(\text{COO}^-)$ , and  $\nu(\text{C}=\text{O})$  in Vit B<sub>3</sub> were shifted to 1041, 1361 and 1627 cm<sup>-1</sup> in Cu-MOF, respectively. This shifting in peaks reveals the coordination between the Cu atom, -COOH and N atom in Vit B<sub>3</sub>, and moreover, the two bands at 1902 and 2415 cm<sup>-1</sup> disappeared in Cu-MOF, which emphasizes that copper and Vit B<sub>3</sub> were coordinated.<sup>38</sup>

### 3.7. Organic reaction

The synthesized Cu/Vit B<sub>3</sub>-MOF has a crystalline structure (see the XRD in Fig. 5), tunable pore topology as in SEM (Fig. 2), and high surface areas. In general, MOFs show a great deal of promise, especially when it comes to catalysis.<sup>39,40</sup> Our research group is motivated to explore new catalytic multicomponent reactions (MCRs) due to the distinctive characteristics of MOFs.<sup>34,41-47</sup> Benzoxanthenones, as previously mentioned, have been used as scaffolding in numerous biological applications. Our focus is on developing a novel, environmentally friendly, and effective catalytic process for the production of these heterocyclic molecules.

The reaction was started with an optimization step by changing the “temperature and solvents” to choose suitable reaction conditions. Finally, the best conditions for the synthesis



**Table 1** Cu-MOF compared with reported catalysts in catalytic activity for one-pot synthesis of **4a**

Entry	Catalyst	Time (min)	Yield (%)
1	Tetrabutyl ammonium fluoride (TBAF)	540	99 (ref. 48)
2	BF <sub>3</sub> · OEt <sub>2</sub>	45	82 (ref. 49)
3	NH <sub>2</sub> SO <sub>3</sub> H	60	67 (ref. 50)
4	[DSTMG][CH <sub>3</sub> COO]	25	70 (ref. 51)
5	Cu/Vit B <sub>3</sub> -MOF	25	90

of **4a** as a model example is a one-pot reaction of one mole of benzaldehyde, one mole of dimedone and one mole of β-naphthol in the presence of the catalytic amount of the prepared MOF at 60–70 °C under solvent-free conditions. Table 1 explains the efficiency of the prepared Cu-MOF compared with that of reported catalysts in the one-pot synthesis of **4a**.

After the reaction optimization step using green solvents, such as water, and comparing it with the solvent-free reaction, the data obtained seems similar (Scheme 1). So, the reaction was explored by verifying the substituent in the aldehydic ring. As an example, aldehyde **3j** reacted with dimedone and 2-naphthol in the presence of the catalytic amount of Cu/Vit B<sub>3</sub>-MOF NPs without solvent at 60–70 °C. Crystallization was used to purify the final product. Elemental and spectral analyses were used to characterize its structure. Reaction times and yields for the final products **4a–j** are reported in Table 2.

A plausible mechanism for the synthesis of tetrahydrobenzo[*a*]xanthenone derivatives using Cu/Vit B<sub>3</sub>-MOF nanoparticles is indicated in Scheme 2. Cu/Vit B<sub>3</sub>-MOF nanoparticles most likely function as a Lewis acid, utilizing a strong coordination bond to enhancement the polarity of the C=O group in the aldehyde and dimedone. *Ortho*-quinone methides (*o*-QMs) intermediate **A** is first produced by the nucleophilic addition of aldehydes and 2-naphthol in the presence of Cu/Vit B<sub>3</sub>-MOF nanoparticles as a catalyst. Following Michael addition of dimedone with *o*-QM, intermediate **B** is created and coordinates to the catalyst to cyclize, accompanied by the loss of H<sub>2</sub>O resulting in product **4h**.

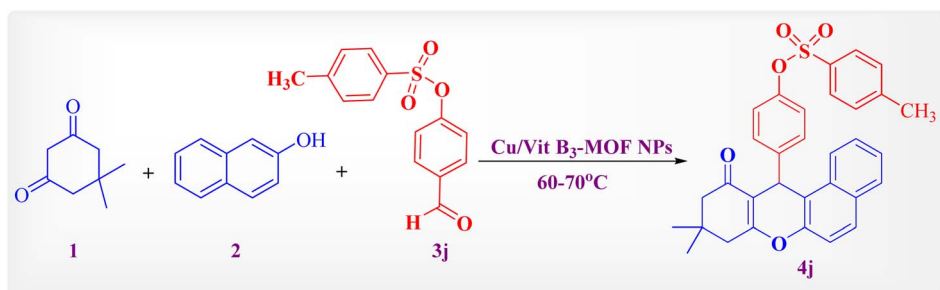
The data obtained in Table 2 is aimed at measuring the efficiency of the catalyst in the synthesis of benzoxanthenones by one-pot reactions. It was necessary to keep two components with no change and change only one component so that we

could evaluate the effect of substituents on the aromatic aldehyde in the reaction. Practical data confirmed that the reaction time is affected by the steric hindrance, and this is acceptable for use related to the tetragonal structure of the prepared MOF catalyst and also the effect of the β-naphthol size. Thus, all the substituted aldehydes take a longer time than the small-sized substituents such as F or unsubstituted aldehydic ring. Finally, the high efficiency of the reaction is interpreted as the role of the catalyst, as explained in the reaction mechanism, where the catalyst raises the polarizing force of the carbonyl groups, and this stimulates the nucleophilic attack.

### 3.8. Molecular docking

In recent years, new types of bacterial infections have spread, such as *Helicobacter pylori*, which is considered one of the most common causes of stomach ulcers and duodenitis and without treatment leads to the formation of stomach cancer. This type is treated with triple therapy consisting of antibiotics such as amoxicillin, clarithromycin (Biaxin®), metronidazole (Flagyl®) and tetracycline, in combination with a proton pump, and antacids. So far, no treatment has been found specifically for this bacterial infection. Therefore, the following information has been presented to find a therapy specialized in eliminating *Helicobacter pylori*. The targeted enzyme type II dehydroquinase (DHQase) plays an important role in the synthesis of some significant bioactive organic compounds, such as tryptophan, tyrosine, phenylalanine, and other aromatic metabolites from shikimate. All these metabolites are very important in bacterial cell life, and the selectivity comes from in the human body where there are other enzymes used in these types of reactions.<sup>52</sup> Using a docking computational method, we can measure the degree of the binding between prepared ligands (**4a–4j**) and target protein active sites in II dehydroquinase (DHQase), and the data obtained can be summarized as follows:

The binding between ligand (**4j**) and active side amino acid residues (Ala79, Leu11, Asp18, Pro19, Arg113, Pro9, His82, Asn10, Thr104, Ile106, His102, Gly78, Leu103, Asn76, Met13, Thr83, Val1001, Phe112, Leu14 and Arg109) firstly can be explained as two-dimensional (Fig. 9). As explained before, the targeted receptor II dehydroquinase (DHQase) is an important transformed enzyme in *Helicobacter pylori*. The presented example gives the promised stacking with the DHQase receptor



**Scheme 1** One-pot synthesis of **4j** as an example for benzoxanthenones derivatives. Conditions: **1** (1 mmol), **2** (1 mmol), **3** (1 mmol), Cu/Vit B<sub>3</sub>-MOF (0.05 g), stirring at 60–70 °C.



Table 2 Cu-MOF catalyzed synthesis of benzoxanthenone derivatives (4a–j)<sup>a</sup>

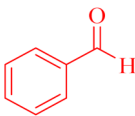
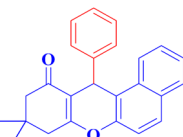
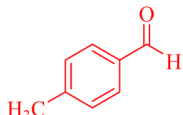
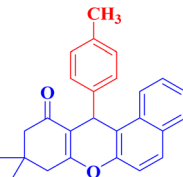
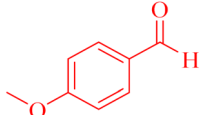
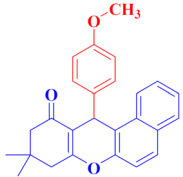
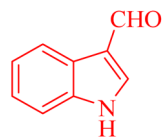
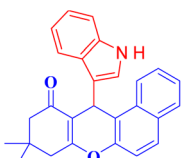
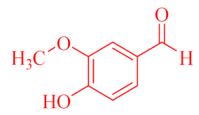
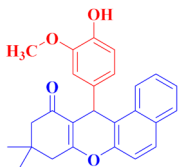
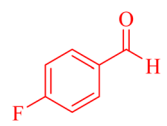
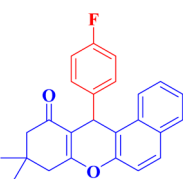
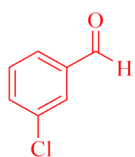
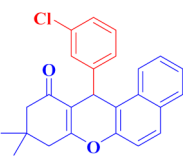
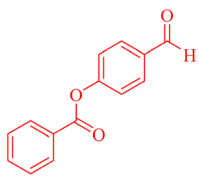
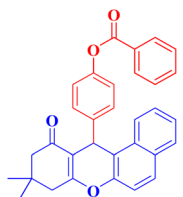
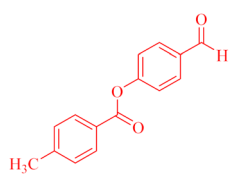
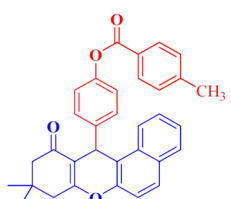
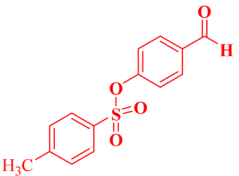
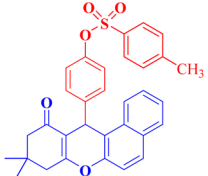
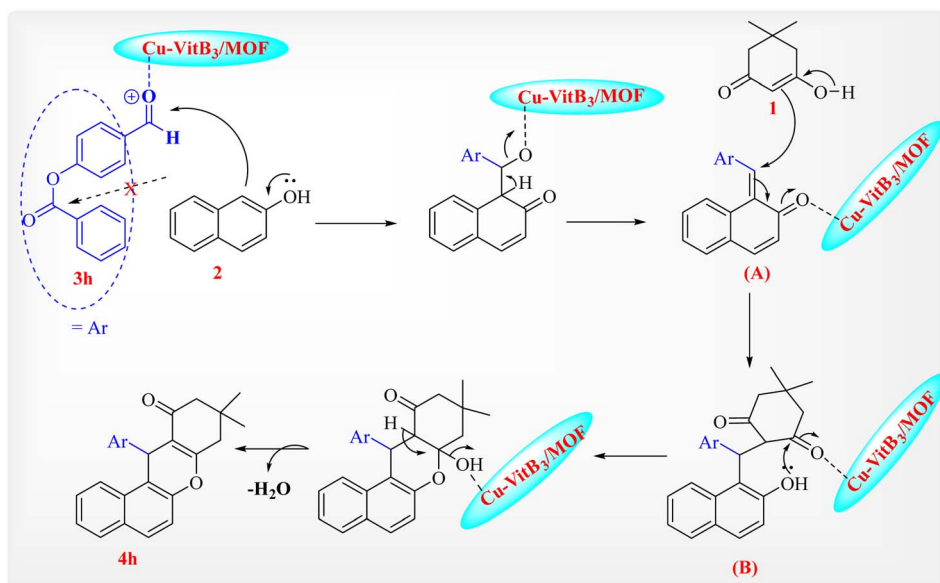
Entry	Aldehyde	Product	Product structure	Time (min)	Yield <sup>b</sup> (%)	Mp <sup>c</sup> (°C)
1		4a		25	90	150–151 <sup>c</sup>
2		4b		40	85	174–176 <sup>c</sup>
3		4c		60	80	205–206 <sup>c</sup>
4		4d		60	85	202–204 <sup>c</sup>
5		4e		50	80	193–194 <sup>c</sup>
6		4f		20	84	184–186 <sup>c</sup>
7		4g		60	88	205–206 <sup>c</sup>
8		4h		50	92	180–182
9		4i		60	90	185–187



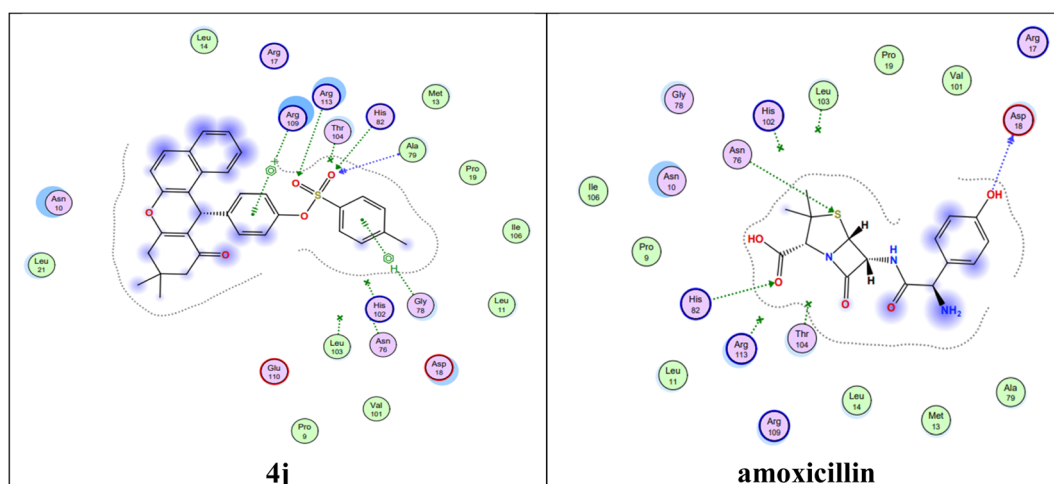
Table 2 (Contd.)

Entry	Aldehyde	Product	Product structure	Time (min)	Yield <sup>b</sup> (%)	Mp <sup>c</sup> (°C)
10		<b>4j</b>		60	90	170–172

<sup>a</sup> Conditions: **1** (1 mmol), **2** (1 mmol), **3** (1 mmol), Cu-MOF (0.05 g), stirring at 60–70 °C. <sup>b</sup> Product yield. <sup>c</sup> Melting points of known cpds match with literature values.<sup>35,36</sup>



Scheme 2 Reaction mechanism suggestion.

Fig. 9 Two-dimensional interaction between **4j** and amoxicillin with *Helicobacter pylori* type II dehydroquinase.



by many electrostatic bonds compared with the reference molecule.

The docking protocol explains that the calculation of energy score by  $\text{kcal mol}^{-1}$  reflects the degree of binding. The data obtained explained that the four ligands from the prepared compounds (**4d**, **4e**, **4h** and **4j**) possess significantly lower energy score values as compared to that of amoxicillin, the reference molecule (Fig. 10). The lower energy scores of the four derivatives (**4d**, **4e**, **4h** and **4j**) were explained by the fact that they can form a greater number of electrostatic bonds, such as “hydrogen bond, dipole–dipole and  $\pi$ – $\pi$  stacking”, compared to those of the reference molecule.

Fig. 11 shows the binding interaction between ligand (**4j**) and the active site in DHQase by a three-dimensional conformation. The data obtained show that at least 6 bonds (explained by dotted lines) can be formed between ligand (**4j**) and the targeted enzyme *Helicobacter pylori* type II dehydroquinase and 4 hydrogen bonds between the sulphonyl group in the ligand and enzyme amino acid residues Arg109, Arg113, His82, and Ala79 with measured bond lengths 1.80, 2.37, and 1.88 and 2.22,

respectively. There are two hydrophobic bonds ( $\pi$ – $\pi$  stacking) between the two-benzene ring in the prepared ligand and enzyme amino acid residue Arg109 and Gly78.

## 4. Conclusion

A copper–Vit B<sub>3</sub> MOF was successfully hydrothermally prepared by an efficient and green method at a nano size. The structure was characterized and illustrated by IR, XRD, SEM, TEM and EDX. The prepared MOF was used in the synthesis of some benzoxanthene derivatives (**4a–4j**). The prepared heteropolycyclic compounds were evaluated as *Helicobacter pylori* type II dehydroquinase inhibitors compared with amoxicillin. The data obtained shows that four derivatives, **4d**, **4e**, **4h** and **4j**, can presented in *Helicobacter pylori* treatment compared with that of amoxicillin.

## Conflicts of interest

There are no conflicts to declare.

## Acknowledgements

The authors extend their appreciation to the Deanship of Scientific Research, King Saud University for funding through the Vice Deanship of Scientific Research Chairs (Drug Exploration and Development Chair). Further, the authors are grateful to Princess Nourah Bint Abdulrahman University, Riyadh, Saudi Arabia for funding this work through Researchers Supporting Project Number (PNURSP2024R35).

## References

- 1 J. Q. Cao, Y. Yao, H. Chen, L. Qiao, Y. Z. Zhou and Y. H. Pei, A New xanthene from *Blumea riparia*, *Chin. Chem. Lett.*, 2007, **18**, 303–305, DOI: [10.1016/j.ccl.2007.01.029](https://doi.org/10.1016/j.ccl.2007.01.029).
- 2 M. Bai, C.-J. Zheng, X.-H. Nong, X.-M. Zhou, Y.-P. Luo and G.-Y. Chen, Four New Insecticidal Xanthene Derivatives from the Mangrove-Derived Fungus *Penicillium* sp. JY246, *Mar. Drugs*, 2019, **17**, 649, DOI: [10.3390/md17120649](https://doi.org/10.3390/md17120649).
- 3 S. N. Richardson, T. K. Nsiama, A. K. Walker, D. R. McMullin and J. D. Miller, Antimicrobial dihydrobenzofurans and xanthenes from a foliar endophyte of *Pinus strobus*, *Phytochemistry*, 2015, **117**, 436–443, DOI: [10.1016/j.phytochem.2015.07.009](https://doi.org/10.1016/j.phytochem.2015.07.009).
- 4 A. Barmak, K. Niknam, G. Mohebbi and H. Pournabi, Antibacterial studies of hydroxyspiro[indoline-3,9-xanthene]trione against spiro[indoline3,9-xanthene]trione and their use as acetyl and butyrylcholinesterase inhibitors, *Microb. Pathog.*, 2019, **130**, 95–99, DOI: [10.1016/j.micpath.2019.03.002](https://doi.org/10.1016/j.micpath.2019.03.002).
- 5 H. N. Hafez, M. I. Hegab, I. S. Ahmed-Farag and A. B. A. El-Gazzar, A facile regioselective synthesis of novel spirothioxanthene and spiro-xanthene-9',2-[1,3,4]thiadiazole derivatives as potential analgesic and anti-inflammatory agents, *Bioorg. Med. Chem. Lett.*, 2008, **18**, 4538–4543, DOI: [10.1016/j.bmcl.2008.07.042](https://doi.org/10.1016/j.bmcl.2008.07.042).

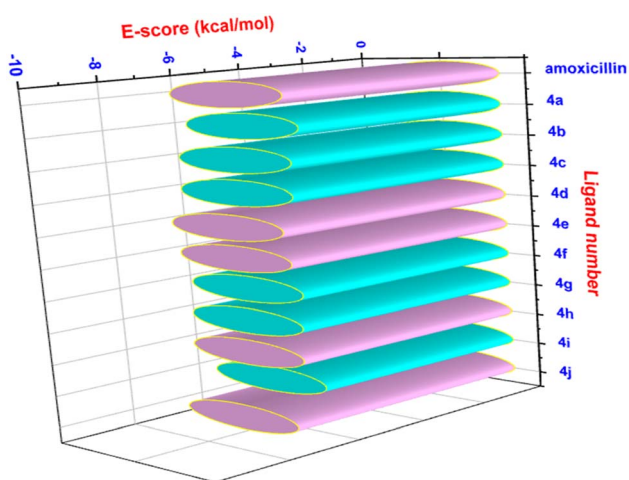


Fig. 10 Energy score of the prepared ligands and amoxicillin and DHQase.

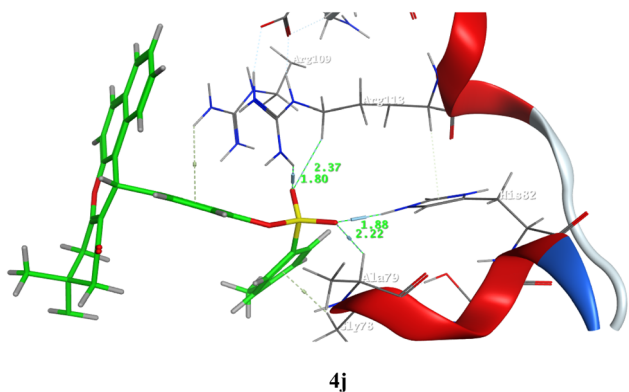


Fig. 11 Three-dimensional interaction between **4j** and *Helicobacter pylori* type II dehydroquinase. Numbers in green refer to the bond length.



- 6 K. V. Sashidhara, A. Kumar, R. P. Dodda and B. A. Kumar, A new iodine catalyzed regioselective synthesis of xanthen synthons, *Tetrahedron Lett.*, 2012, **53**, 3281–3283, DOI: [10.1016/j.tetlet.2012.04.061](https://doi.org/10.1016/j.tetlet.2012.04.061).
- 7 A. Ilangoan, K. Anandhan, K. M. Prasad, P. Vijayakumar, R. Renganathan, D. A. Ananth and T. Sivasudha, Synthesis, DNA-binding study, and antioxidant activity of 14-aryl-14H-dibenzo[a,j]xanthene derivatives, *Med. Chem. Res.*, 2015, **24**, 344–355, DOI: [10.1007/s00044-014-1124-8](https://doi.org/10.1007/s00044-014-1124-8).
- 8 M. Kaya, E. Demir and H. Bekci, Synthesis, characterization and antimicrobial activity of novel xanthene sulfonamide and carboxamide derivatives, *J. Enzyme Inhib. Med. Chem.*, 2013, **28**, 885–893, DOI: [10.3109/14756366.2012.692087](https://doi.org/10.3109/14756366.2012.692087).
- 9 A. Kumar, L. Rout, L. S. K. Achary, R. S. Dhaka and P. Dash, Greener Route for Synthesis of Aryl and Alkyl-14H-dibenzo [a,j] xanthenes using Graphene Oxide-Copper Ferrite Nanocomposite as a Recyclable Heterogeneous Catalyst, *Sci. Rep.*, 2017, **7**, 42975, DOI: [10.1038/srep42975](https://doi.org/10.1038/srep42975).
- 10 T. S. Jin, L. B. Liu, Y. Zhao and T. S. Li, Clean Synthesis of Compounds Containing Two 4H-Pyrans or Two Tetraketones in Aqueous Media, *Synth. Commun.*, 2005, **35**, 2379–2385, DOI: [10.1080/00397910500187779](https://doi.org/10.1080/00397910500187779).
- 11 K. Chibale, M. Visser, D. Van Schalkwyk, P. J. Smith, A. Saravanamuthu and A. H. Fairlamb, Exploring the potential of xanthene derivatives as trypanothione reductase inhibitors and chloroquine potentiating agents, *Tetrahedron*, 2003, **59**, 2289–2296, DOI: [10.1016/S0040-4020\(03\)00240-0](https://doi.org/10.1016/S0040-4020(03)00240-0).
- 12 R. D. Bongard, M. Lepley, A. Gastonguay, R. R. Syrlybaeva, M. R. Talipov, R. A. Jones Lipinski, N. R. Leigh, J. Brahmabhatt, R. Kutty, R. Rathore, R. Ramchandran and D. S. Sem, Discovery and characterization of halogenated xanthene inhibitors of DUSP5 as potential photodynamic therapeutics, *J. Photochem. Photobiol., A*, 2019, **375**, 114–131, DOI: [10.1016/j.jphotochem.2019.01.005](https://doi.org/10.1016/j.jphotochem.2019.01.005).
- 13 D. Lee, K. M. K. Swamy, J. Hong, S. Lee and J. Yoon, A rhodamine-based fluorescent probe for the detection of lysosomal pH changes in living cells, *Sens. Actuators, B*, 2018, **266**, 416–421, DOI: [10.1016/j.snb.2018.03.133](https://doi.org/10.1016/j.snb.2018.03.133).
- 14 Y. Khairy, M. I. Mohammed, H. I. Elsaedy and I. S. Yahia, Synthesis, optical limiting and properties of rhodamine B-doped PMMA polymeric films/glass substrate: new trends in polymeric composites, *Optik*, 2020, **212**, 164687, DOI: [10.1016/j.ijleo.2020.164687](https://doi.org/10.1016/j.ijleo.2020.164687).
- 15 A. A. Ali, M. Konwar, M. Chetia and D. Sarma, [Bmim]OH mediated Cu-catalyzed azide–alkyne cycloaddition reaction: a potential green route to 1,4-disubstituted 1,2,3-triazoles, *Tetrahedron Lett.*, 2016, **57**, 5661–5665, DOI: [10.1016/j.tetlet.2016.11.014](https://doi.org/10.1016/j.tetlet.2016.11.014).
- 16 IUPAC, *Compendium of Chemical Terminology*, Blackwell Scientific Publications, Oxford, 2nd edn, 1997, <https://publications.iupac.org/publications/books/author/mcnaught.html>.
- 17 M. Zhang, Y.-H. Liu, Z.-R. Shang, H.-C. Hu and Z.-H. Zhang, Supported molybdenum on graphene oxide/Fe<sub>3</sub>O<sub>4</sub>: an efficient, magnetically separable catalyst for one-pot construction of spiro-oxindole dihydropyridines in deep eutectic solvent under microwave irradiation, *Catal. Commun.*, 2017, **88**, 39–44, DOI: [10.1016/j.catcom.2016.09.028](https://doi.org/10.1016/j.catcom.2016.09.028).
- 18 M.-N. Chen, L.-P. Mo, Z.-S. Cui and Z.-H. Zhang, Magnetic nanocatalysts: synthesis and application in multicomponent reactions, *Curr. Opin. Green Sustainable Chem.*, 2019, **15**, 27–37, DOI: [10.1016/j.cogsc.2018.08.009](https://doi.org/10.1016/j.cogsc.2018.08.009).
- 19 M. A. Mannaa, M. R. Mlahi, A. AL Maofari, A. I. Ahmed and S. M. Hassan, Synthesis of Highly Efficient and Recyclable Bimetallic Co<sub>x</sub>–Fe<sub>1–x</sub>–MOF for the Synthesis of Xanthan and Removal of Toxic Pb<sup>2+</sup> and Cd<sup>2+</sup> Ions, *ACS Omega*, 2023, **8**, 26379–26390, DOI: [10.1021/acsomega.3c02911](https://doi.org/10.1021/acsomega.3c02911).
- 20 H. Ghafuri, F. Ganjali and P. Hanifehnejad, Cu.BTC MOF as a Novel and Efficient Catalyst for the Synthesis of 1,8-Dioxo-octa-hydro Xanthene, *Chem. Process*, 2020, **1**, 2, DOI: [10.3390/ecsoc-24-08359](https://doi.org/10.3390/ecsoc-24-08359).
- 21 C. P. Raptopoulou, Metal-organic frameworks: synthetic methods and potential applications, *Materials*, 2021, **14**, 310, DOI: [10.3390/ma14020310](https://doi.org/10.3390/ma14020310).
- 22 H. Furukawa, K. E. Cordova, M. O’Keeffe and O. M. Yaghi, The chemistry and applications of metal-organic frameworks, *Science*, 2013, **341**, 1230444, DOI: [10.1126/science.1230444](https://doi.org/10.1126/science.1230444).
- 23 L. Andre, N. Desbois, C. P. Gros and S. Brandes, Porous materials applied to biomarker sensing in exhaled breath for monitoring and detecting non-invasive pathologies, *Dalton Trans.*, 2020, **49**, 15161–15170, DOI: [10.1039/d0dt02511a](https://doi.org/10.1039/d0dt02511a).
- 24 F. A. Paz, J. Klinowski, S. M. Vilela, J. P. Tome, J. A. Cavaleiro and J. Rocha, Ligand design for functional metal-organic frameworks, *Chem. Soc. Rev.*, 2012, **41**, 1088–1110, DOI: [10.1039/c1cs15055c](https://doi.org/10.1039/c1cs15055c).
- 25 S. Noro, R. Kitaura, M. Kondo, S. Kitagawa, T. Ishii, H. Matsuzaka and M. Yamashita, Framework engineering by anions and porous functionalities of Cu(II)/4,4'-bpy coordination polymers, *J. Am. Chem. Soc.*, 2002, **124**, 2568–2583, DOI: [10.1021/ja0113192](https://doi.org/10.1021/ja0113192).
- 26 P. Li, N. A. Vermeulen, C. D. Malliakas, D. A. Gomez-Gualdrón, A. J. Howarth, B. L. Mehdi, A. Dohnalkova, N. D. Browning, M. O’Keeffe and O. K. Farha, Bottom-up construction of a superstructure in a porous uranium-organic crystal, *Science*, 2017, **356**, 624–627, DOI: [10.1126/science.aam7851](https://doi.org/10.1126/science.aam7851).
- 27 F. R. Fortea-Perez, M. Mon, J. Ferrando-Soria, M. Boronat, A. Leyva-Perez, A. Corma, J. M. Herrera, D. Osadchii, J. Gascon, D. Armentano and E. Pardo, The MOF-driven synthesis of supported palladium clusters with catalytic activity for carbene-mediated chemistry, *Nat. Mater.*, 2017, **16**, 760–766, DOI: [10.1038/nmat4910](https://doi.org/10.1038/nmat4910).
- 28 R. Li, S. Alomari, T. Islamoglu, O. K. Farha, S. Fernando, S. M. Thagard, T. M. Holsen and M. Wriedt, Systematic study on the removal of per- and polyfluoroalkyl substances from contaminated groundwater using metal-organic frameworks, *Environ. Sci. Technol.*, 2021, **55**, 15162–15171, DOI: [10.1021/acs.est.1c03974](https://doi.org/10.1021/acs.est.1c03974).
- 29 Z. Jiang, X. Xu, Y. Ma, H. S. Cho, D. Ding, C. Wang, J. Wu, P. Oleynikov, M. Jia, J. Cheng, Y. Zhou, O. Terasaki,



- T. Peng, L. Zan and H. Deng, Filling metal-organic framework mesopores with TiO<sub>2</sub> for CO<sub>2</sub> photoreduction, *Nature*, 2020, **586**, 549–554, DOI: [10.1038/s41586-020-2738-2](https://doi.org/10.1038/s41586-020-2738-2).
- 30 M. Viciano-Chumillas, M. Mon, J. Ferrando-Soria, A. Corma, A. Leyva-Pérez, D. Armentano and E. Pardo, Metal-organic frameworks as chemical nanoreactors: synthesis and stabilization of catalytically active metal species in confined spaces, *Acc. Chem. Res.*, 2020, **53**, 520–531, DOI: [10.1021/acs.accounts.9b00609](https://doi.org/10.1021/acs.accounts.9b00609).
- 31 R. J. Young, M. T. Huxley, E. Pardo, N. R. Champness, C. J. Sumby and C. J. Doonan, Isolating reactive metal-based species in metal-organic frameworks—viable strategies and opportunities, *Chem. Sci.*, 2020, **11**, 4031–4050, DOI: [10.1039/D0SC00485E](https://doi.org/10.1039/D0SC00485E).
- 32 Y. Li, H. Choi, K. Leung, F. Jiang, D. Y. Graham and W. K. Leung, Global prevalence of *Helicobacter pylori* infection between 1980 and 2022: a systematic review and meta-analysis, *Lancet Gastroenterol. Hepatol.*, 2023, **8**, 553–564, DOI: [10.1016/S2468-1253\(23\)00070-5](https://doi.org/10.1016/S2468-1253(23)00070-5).
- 33 J. R. McConaghy, A. Decker and S. Nair, Peptic ulcer disease and *H. pylori* infection: common questions and answers, *Am. Fam. Physician*, 2023, **107**, 165–172, <https://www.binasss.sa.cr/int23/9.pdf>.
- 34 G. E. Said, M. Tarek, A. A. Zen, A. A. Almehizia, A. M. Naglah and T. K. Khatab, Novel Cobalt/vitamin B3 metal-organic framework as nano-catalyst in synthesis of some new bis-indole derivatives with stacking validation towards *Salmonella* DNA, *J. Organomet. Chem.*, 2024, **1008**, 123074, DOI: [10.1016/j.jorganchem.2024.123074](https://doi.org/10.1016/j.jorganchem.2024.123074).
- 35 F. Diwan, M. Mohsin, M. Shaikh, P. Dixit and M. Farooqui, Tetrabutyl ammonium hydrogen sulphate (TBAHS) Catalyzed Convenient and Greener Synthesis of Tetrahydrobenzo[*a*]xanthene-11-ones, *Chem. Biol. Interface*, 2019, **9**, 71–82, <https://cbijournal.com/paper-archive/january-february-2019-vol-1/Research-Paper-6-tetrabutyl-ammonium-hydrogen-sulphate-tbahs-catalyzed-convenient-and-greener-synthesis.pdf>.
- 36 H.-J. Wang, X.-Q. Ren, Y.-Y. Zhang and Z.-H. Zhang, Synthesis 12-Aryl or 12-Alkyl-8,9,10,12-tetrahydrobenzo[*a*]xanthene-11-one Derivatives Catalyzed by Dodecatungstophosphoric Acid, *J. Braz. Chem. Soc.*, 2009, **20**, 1939–1943, DOI: [10.1590/S0103-50532009001000025](https://doi.org/10.1590/S0103-50532009001000025).
- 37 I. W. Almanassra, L. Jaber, A. Chatla, A. Abushawish, A. Shanableh and M. A. Atieh, Unveiling the relationship between MOF porosity, particle size, and polyethersulfone membranes properties for efficient decontamination of dye and organic matter, *Chem. Eng. J.*, 2023, **144616**, 1385–8947, DOI: [10.1016/j.cej.2023.144616](https://doi.org/10.1016/j.cej.2023.144616).
- 38 M. K. Trivedi, A. Branton, D. Trivedi, G. Nayak, K. Bairwa and S. Jan, Spectroscopic Characterization of Disulfiram and Nicotinic Acid after Biofield Treatment, *J. Anal. Bioanal. Tech.*, 2015, **6**, 2, DOI: [10.4172/2155-9872.1000265](https://doi.org/10.4172/2155-9872.1000265).
- 39 Y. Z. Chen, R. Zhang, L. Jiao and H. L. Jiang, Metal-organic framework-derived porous materials for catalysis, *Coord. Chem. Rev.*, 2018, **362**, 1–23, DOI: [10.1016/j.ccr.2018.02.008](https://doi.org/10.1016/j.ccr.2018.02.008).
- 40 Q. Yang, Q. Xu and H. L. Jiang, Metal-organic frameworks meet metal nanoparticles: synergistic effect for enhanced catalysis, *Chem. Soc. Rev.*, 2017, **46**, 4774–4808, DOI: [10.1039/c6cs00724d](https://doi.org/10.1039/c6cs00724d).
- 41 T. K. Khatab, A. M. Abdelghanyb and H. A. Soliman, V<sub>2</sub>O<sub>5</sub> based quadruple nano-perovskite as a new catalyst for the synthesis of bis and tetrakis heterocyclic compounds, *Appl. Organomet. Chem.*, 2019, **33**, e4783, DOI: [10.1002/aoc.4783](https://doi.org/10.1002/aoc.4783).
- 42 T. K. Khatab, A. S. Hassan and T. S. Hafez, V<sub>2</sub>O<sub>5</sub>/SiO<sub>2</sub> as an efficient catalyst in the synthesis of 5-aminopyrazole derivatives under solvent free condition, *Bull. Chem. Soc. Ethiop.*, 2019, **33**, 135–142, DOI: [10.4314/bcse.v33i1.13](https://doi.org/10.4314/bcse.v33i1.13).
- 43 H. A. Soliman and T. K. Khatab, V<sub>2</sub>O<sub>5</sub>/SiO<sub>2</sub> as a Heterogeneous Catalyst in the Synthesis of bis(indolyl) metanes Under Solvent Free Condition, *Silicon*, 2018, **10**, 703–708, DOI: [10.1007/s12633-016-9515-8](https://doi.org/10.1007/s12633-016-9515-8).
- 44 A. M. Abdelghany, H. A. Soliman and T. K. Khatab, Biosynthesized selenium nanoparticles as a new catalyst in the synthesis of quinazoline derivatives in pentacyclic system with docking validation as (TRPV1) inhibitor, *J. Organomet. Chem.*, 2021, **944**, 121847, DOI: [10.1016/j.jorganchem.2021.121847](https://doi.org/10.1016/j.jorganchem.2021.121847).
- 45 E. Abdel-Latif, T. K. Khatab, A. Fekri and M. E. Khalifa, Synthesis of New Binary Thiazole-Based Heterocycles and Their Molecular Docking Study as COVID-19 Main Protease (Mpro) Inhibitors, *Russ. J. Gen. Chem.*, 2021, **91**, 1767–1773, DOI: [10.1134/S1070363221090231](https://doi.org/10.1134/S1070363221090231).
- 46 N. Shaker, E. M. Kandil, Y. Osama, T. K. Khatab and M. E. Khalifa, ZnCl<sub>2</sub>/SiO<sub>2</sub> as a New Catalyst for the Eco-Friendly Synthesis of *N*-Thiocarbamoyl Pyrazoles and Thiosemicarbazones with Antioxidant and Molecular Docking Evaluation as (UppS) Inhibitor, *Curr. Org. Chem.*, 2021, **25**, 2037–2044, DOI: [10.2174/1385272825666210809142341](https://doi.org/10.2174/1385272825666210809142341).
- 47 T. K. Khatab, E. M. Kandil, D. E. Elsefy and A. A. El-Mekabaty, one-pot multicomponent catalytic synthesis of new 1*H*-Pyrazole-1-Carbothioamide derivatives with molecular docking studies as COX-2 inhibitors, *Biointerface Res. Appl. Chem.*, 2021, **11**, 13779–13789, DOI: [10.33263/BRIAC116.1377913789](https://doi.org/10.33263/BRIAC116.1377913789).
- 48 S. Gao, C. H. Tsai and C.-F. Yao, A Simple and Green Approach for the Synthesis of Tetrahydrobenzo[*a*]xanthene-11-one Derivatives Using Tetrabutyl Ammonium Fluoride in Water, *Synlett*, 2009, **6**, 0949–0954, DOI: [10.1055/s-0028-1088214](https://doi.org/10.1055/s-0028-1088214).
- 49 A. Sethukumar, M. M. Chandy, B. A. Prakasam and R. Pallegogu, Synthesis and spectral studies on some tetrahydrobenzoxanthene-11-ones: crystal and molecular structure of 9,9-dimethyl-12-(2-nitrophenyl)-8,9,10,12-tetrahydrobenzo[*a*]xanthene-11-one, *Struct. Chem.*, 2011, **22**, 671–680, DOI: [10.1007/s11224-011-9737-8](https://doi.org/10.1007/s11224-011-9737-8).
- 50 H. Zang, Y. Zhang, B. Cheng, W. Zhang, X. Xu and Y. Ren, An Efficient and Green One-pot Synthesis of 12-Aryl-8, 9, 10, 12-tetrahydrobenzo [a] xanthene-11-one Derivatives Promoted by Sulfamic Acid in [BMIM] BF<sub>4</sub> Ionic Liquid, *Chin. J. Chem.*, 2012, **30**, 362–366, DOI: [10.1002/cjoc.201180488](https://doi.org/10.1002/cjoc.201180488).



- 51 A. K. Dutta, P. Gogoi, S. Saikia and R. Borah, N,N-disulfo-1,1,3,3-tetramethylguanidinium carboxylate ionic liquids as reusable homogeneous catalysts for multicomponent synthesis of tetrahydrobenzo[*a*]xanthene and tetrahydrobenzo[*a*]acridine derivatives, *J. Mol. Liq.*, 2017, **225**, 585–591, DOI: [10.1016/j.molliq.2016.11.112](https://doi.org/10.1016/j.molliq.2016.11.112).
- 52 D. A. Robinson, K. A. Stewart, N. C. Price, P. A. Chalk, J. R. Coggins and A. J. Laphorn, Crystal Structures of Helicobacter pylori Type II Dehydroquinase Inhibitor Complexes: New Directions for Inhibitor Design, *J. Med. Chem.*, 2006, **49**, 1282–1290, DOI: [10.1021/jm0505361](https://doi.org/10.1021/jm0505361).

